

Higgs-boson decay to four fermions including a single top quark below $t\bar{t}$ threshold

Heath Pois*

*Center for Theoretical Physics, Department of Physics, Texas A&M University, College Station, Texas 77843-4242
and Astroparticle Physics Group, Houston Advanced Research Center (HARC), The Woodlands, Texas 77381*

Thomas J. Weiler†

Department of Physics and Astronomy, Vanderbilt University, Nashville, Tennessee 37235

Tzu Chiang Yuan‡

Department of Physics and Astronomy, Northwestern University, Evanston, Illinois 60208

(Received 4 November 1991; revised manuscript received 2 November 1992)

The rare decay modes Higgs boson \rightarrow four light fermions and Higgs boson \rightarrow single top quark + three light fermions for $m_t < M_H < 2m_t$ are presented, and phenomenologically interpreted. The angular correlation between fermion planes is presented as a test of the spin and intrinsic parity of the Higgs particle. In Higgs-boson decay to a single top quark, two tree-level graphs contribute in the standard model (SM); one couples the Higgs boson to W^+W^- ($\sim gM_W$), and one to $t\bar{t}$ ($\sim g_{\text{top Yukawa}} = m_t/246$ GeV). The large Yukawa coupling for $m_t > 100$ GeV makes the second amplitude competitive or dominant for most M_H, m_t values. Thus the Higgs-boson decay rate to a single top quark directly probes the SM universal mechanism generating both gauge-boson and fermion masses, and offers a means to infer the Higgs-boson- $t\bar{t}$ Yukawa coupling when $H \rightarrow t\bar{t}$ is kinematically disallowed. We find that the modes $pp \rightarrow Xt\bar{t}(H \rightarrow t\bar{b}W^{(*)})$ at the Superconducting Super Collider, and $e^+e^- \rightarrow Z$ or $\nu\bar{\nu} + (H \rightarrow t\bar{b}W^{(*)})$ at future high-energy, high-luminosity colliders, may be measurable if $2m_t$ is not too far above M_H . We classify nonstandard Higgs-bosons as gaugeophobic, fermiophobic, or fermiophilic, and discuss the Higgs boson \rightarrow single top-quark rates for these classes.

PACS number(s): 14.80.Gt, 13.85.Qk

I. INTRODUCTION

The existence of a Higgs scalar particle, or the onset of new physics at a few TeV or less, is a virtually guaranteed happenstance in particle physics [1]. Either possibility provides a foundation for the electroweak unification and the generation of masses. Of the two, the simpler possibility is the existence of the Higgs particle. Accordingly, a tremendous amount of energy has been, and continues to be, devoted to theoretical and experimental searches for signatures of the Higgs boson [2]. The four experiments at the CERN e^+e^- collider LEP have recently placed a lower bound of $M_H \sim 57$ GeV at 95% C.L. for a standard model (SM) Higgs boson [3]. With regard to the top-quark mass, a direct SM lower bound of $m_t \sim 89$ GeV has also been obtained from the Collider Detector at Fermilab (CDF) experiment [4].

Indirect SM upper bounds for m_t and M_H can be predicted by the theory based on quantum loop phenomenology. It is well known that heavy top-quark loop corrections to certain low-energy and electroweak (EW) observ-

ables (for example, the ρ parameter) are proportional to m_t^2 , and thus the quantum effects are quite sensitive to m_t . The SM consistency of all the low-energy experimental data requires $m_t < 182$ GeV at 95% C.L., with a central value of $m_t = 125 \pm 30$ GeV [5]. On the other hand, the mass dependence of a heavy Higgs loop correction varies as $\ln M_H^2$ in the SM. This is the famous one-loop “screening rule” first recognized by Veltman [6]. Since the dependence of quantum loop effects on the heavy Higgs boson is only logarithmic, low-energy observables are not very sensitive to M_H . However, recent analysis [7] indicates that a weak upper bound ($M_H \sim 300\text{--}500$ GeV) for the SM Higgs boson can be deduced from current low-energy experimental data, which is suggestive of a “light” Higgs boson. In models with a broken supersymmetry, the tree-level mass of the lightest Higgs boson generally lies below the Z mass [2]. However, the large radiative corrections to the Higgs-boson masses due to a heavy top quark [8] may alter this situation significantly.

Finding a signature for an “intermediate-mass” Higgs ($M_W < M_H < 2M_Z$) is particularly problematical. It appears that rare decay modes of the Higgs boson such as $H \rightarrow Z\gamma, \gamma\gamma, \tau^+\tau^-, b\bar{b}, \Theta\gamma$ offer the greatest promise for providing an experimental signature of the particle’s existence [9]. The decay of a Higgs boson with a mass above the two- W threshold is dominantly to two W ’s, and so one might believe that a Higgs boson with a mass not

*Electronic address: pois@tamphys

†Electronic address: weilertj@uclrvax

‡Present address: Department of Physics, University of California at Davis, CA 95616. Electronic address: nuhep::yuant

too far below twice the W mass may have a significant branching fraction to decay through WW^* or W^*W^* intermediate states (W^* denotes a virtual W).

Keung and Marciano [10] have shown that for a standard model Higgs boson with mass below but near the two- W threshold, the branching ratio for the decay $H \rightarrow WW^*$ becomes significant; in fact, this decay mode dominates all others if the decay to $t\bar{t}$ is kinematically forbidden (i.e., $M_H < 2m_t$). Barger *et al.* [11] have considered the $W^*W^* \rightarrow$ four-fermion decay mode in the massless fermion limit, and have made a thorough study of the Superconducting Super Collider (SSC) signal and backgrounds. Their conclusion is that only if $m_t, M_H > 150$ GeV will the decay signal be seen above the $t\bar{t} \rightarrow W\bar{b}Wb$ and W continuum background channels.

Our results here are complementary to the work in [11], and extend that work by including a single massive top quark in the final state. As in [11], we allow both W 's to be virtual, and let phase space optimize the sharing of virtuality between the two W 's. Our exact results for Higgs boson \rightarrow four fermions allow us to exhibit the correlations among final fermion energies and angles that test the presumably scalar nature of the parent Higgs particle. As an example of final-state correlations, we display the dependence of the decay on the angle between the decay planes defined for each vector boson. The analogous azimuthal angular dependence for the process pion $\rightarrow e^+e^-e^+e^-$ was calculated over thirty years ago [12], and ultimately provided the signature distinguishing between a scalar and a pseudoscalar ‘‘pion’’ [13].

In Sec. II we present our result for the massless fermion limit (which agrees with the result in [11]), and we discuss a class of nonstandard Higgs bosons which do not couple directly to fermions. Such ‘‘fermiophobic’’ Higgs bosons decay through loops to two fermions, or through two gauge bosons to four fermions. The ‘‘fermiophobic’’ Higgs branching ratio to four fermions is large, even if mass kinematics require both gauge bosons to be virtual; a calculation of this branching ratio requires the exact formulas presented in this paper. In Sec. III we define the asymmetry parameters relevant to the angular correlations between the fermion planes, and explore the M_H and virtual gauge-boson mass dependence of these parameters.

In Sec. IV we exhibit the rate for the tree-level decay of the Higgs to a single heavy quark (e.g., top) plus three light fermions. Since the Higgs particle has a direct Yukawa coupling to fermions which scales with the fermion mass, this latter calculation includes a second graph with a potentially large contribution to the amplitude, and therefore provides an important contrast to the massless fermion case. We find that due to the large Yukawa coupling for large m_t , the branching ratio to single top quark (e.g., $H \rightarrow t\bar{b}s\bar{c}$) can be almost competitive with the dominant massless fermion decay mode $H \rightarrow WW \rightarrow 4f$, and is certainly competitive with the rare $H \rightarrow \gamma\gamma, Z\gamma, b\bar{b}, \tau^+\tau^-$ decay modes for a range of M_H, m_t values. In Sec. V, we present a brief discussion of the signature and backgrounds for the $H \rightarrow tbW^*$ mode. We argue that the signal may be detectable at hadron colliders for Higgs bosons produced in association with a $t\bar{t}$ pair,

and at future high-energy, high-luminosity e^+e^- colliders. Interesting nonstandard Higgs models are classified in Sec. VI, and the branching ratios to single top quark of these baroque Higgs bosons are discussed. We conclude in Sec. VII. Detailed formulas for the decay of a Higgs boson to four fermions, including the massive heavy top, are collected in an Appendix.

II. HIGGS DECAY TO FOUR MASSLESS FERMIONS

For $H \rightarrow WW, ZZ \rightarrow 4f$ (where the W 's and Z 's may be real or virtual), the relevant Feynman diagram when $m_f = 0$ shown in Fig. 1(a); Fig. 1(b) obviously does not contribute in the massless limit to the SM Higgs boson due to the vanishing Yukawa coupling. (See, however, Sec. VI for nonstandard Higgs bosons.) The result for the Higgs width to four fermions is presented in the Appendix. The differential width is symmetric in the invariant masses Q_1^2 and Q_2^2 of the W or Z gauge bosons, and we show the gauge-boson mass spectrum in Fig. 2 for the process $H \rightarrow WW \rightarrow u\bar{d}s\bar{c} + \bar{u}d\bar{s}c$. One can observe that once $M_H > M_W$, a bimodal distribution results. The twin peaks correspond to one or the other W being on shell; for invariant mass values M_{inv} between the peaks, kinematics requires both W 's to be off shell. It is clear that the relative contribution with both W 's off shell is small for an intermediate-mass Higgs. This observation is borne out in a comparison between the exact four fermion width and the one-gauge-boson on-shell (OGBOS) approximate width [10], which is obtained by replacing one of the Breit-Wigner factors $[(Q^2 - M_V^2)^2 + M_V^2\Gamma_V^2]^{-1}$ in the decay width with the narrow-width approximate (NWA) form $\pi\delta(Q^2 - M_V^2)/M_V\Gamma_V$. In agreement with [11], we find that putting one W on shell is a good approximation to the total decay rate for $M_H > 100$ GeV. For Higgs decay through two Z 's, we find that putting one Z on shell approximates well the true decay rate if $M_H > 115$ GeV. In conclusion, we find that the rate for a SM Higgs particle to decay to four fermions is a percent of that for decay to $b\bar{b}$, for $M_H \sim 100$ GeV, and falls rapidly for lighter Higgs masses; for $M_H > 100$ GeV, the OGBOS approximation gives an accurate rate.

A bit of caution is required when applying the NWA

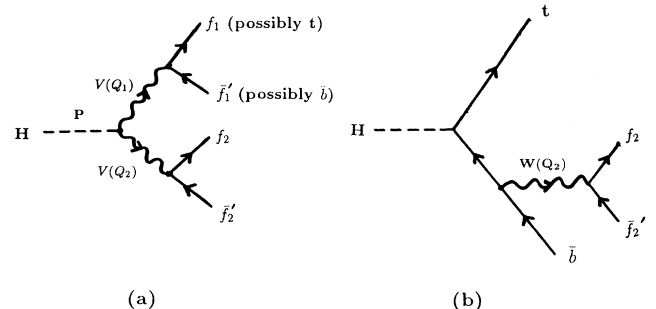


FIG. 1. Feynman diagrams for Higgs-boson decay to four fermions. (a) is the gauge coupling contribution; (b) is the Yukawa contribution in the case of a massive fermion. V is a generic symbol for either W or Z gauge bosons.

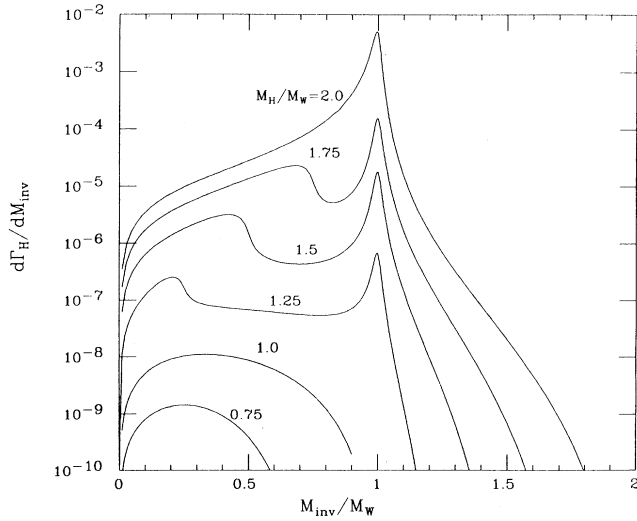


FIG. 2. Differential decay rate for $H \rightarrow u\bar{d}s\bar{c} + \bar{u}d\bar{s}c$ vs the scaled W -invariant mass M_{inv}/M_W for various scaled Higgs masses M_H/M_W .

to the Breit-Wigner integrals of Eq. (A21). If one Breit-Wigner integral is replaced by the NWA δ function, a multiplicative factor of 2 must be introduced to account for the probability for either W to be on shell. Above the two- W threshold, this factor of 2 must be removed since one W on shell no longer precludes the possibility of the second W also being on shell. If Eq. (A21) is used without approximation, there is no need to concern oneself with this extra counting.

The four-fermion mode becomes particularly interesting in models where the two-fermion modes are suppressed at the tree level. Recall that in the SM with three families of quarks and leptons, the Higgs doublet plays a double role of generating masses for both the gauge sector and fermion sector. In fact, there is a third role: the vacuum expectation value (VEV) of the Higgs field breaks not only the $SU(2) \times U(1)$ gauge symmetry but also the flavor symmetry $[U(3)]^5$ (the three copies of the five fields $l_L, q_L, e_R, u_R,$ and d_R). The Higgs mechanism, originally employed to give nonzero masses to the gauge bosons while maintaining a renormalizable theory, may not be the source of the fermion masses or the flavor symmetry breaking. The independent generation of fermion masses and gauge-boson masses is conceptually possible [14]. A suppression of the Higgs couplings to fermions is easily enforced by introducing a discrete $\phi \rightarrow -\phi$ symmetry; the symmetry forbids Yukawa couplings [15]. We call the resulting Higgs fields “fermiophobic,” for although the fields couple to the gauge bosons at tree level, their coupling to fermions occurs only through loops and scalar field mixing. (The loop and mixing-induced couplings are allowed since $\langle \phi \rangle \neq 0$ breaks the discrete symmetry.)

It is a logical possibility then that the sole Higgs particle introduced in the standard model is itself fermiophobic. If so, the rate for a Higgs of intermediate mass to decay to four fermions via two virtual gauge bosons [Fig. 1(a)] competes favorably with all other decays, namely,

Higgs \rightarrow two fermions through scalar mixing and/or loop graphs, Higgs $\rightarrow \gamma\gamma$, or γZ through a W or charged-Higgs loop, and Higgs $\rightarrow gg$ through one loop and mixing or through two loops. In fact, the decay rate to four fermions exceeds the rate to $\gamma\gamma$ or γZ if the Higgs mass exceeds 75 GeV. Branching ratios for a fermiophobic Higgs may be inferred from the SM branching ratios presented in Fig. 2 of Ref. [11]. If an intermediate-mass Higgs is discovered, a comparison of its two-fermion decay rate to its four-fermion or two-photon rate will immediately provide important information on the mechanism(s) of mass generation [16].

III. ANGULAR CORRELATIONS BETWEEN THE FERMION PLANES

Next we turn to the correlations among the final state of four massless fermions implied by the matrix element of Eq. (A4). The reader may recall that parity conservation implies that the two photons resulting from a scalar-particle decay have parallel polarization directions, while the photons from a decaying pseudoscalar particle have perpendicular polarizations [17]. A similar result holds for decay of scalar and pseudoscalar bosons to two Z 's or two W 's with momenta Q_1 and Q_2 and polarization vectors $\epsilon_1^\mu(\lambda)$ and $\epsilon_2^\nu(\lambda')$. The matrix element is linear in the two polarization vectors. In the case of an even-parity Higgs field surviving spontaneous symmetry breaking, the decay proceeds at the tree level with the two polarization vectors contracted $\epsilon_1(\lambda) \cdot \epsilon_2(\lambda')$, which tells us that the two gauge bosons emerge with the same linear polarization. In a helicity basis, the two gauge bosons emerge with the same helicity. For massive gauge bosons, there are of course three physical polarizations, and a fourth “scalar” polarization for off-shell vector bosons which vanishes when coupled to a conserved current. In the case of the odd-parity neutral pseudoscalar decay, CP invariance of the gauge-boson and scalar-boson sectors is sufficient to ensure no tree-level coupling [2]; the process is loop induced with $\phi F\bar{F}$ being the lowest-dimensional operator, just as in the $\pi^0 \rightarrow \gamma\gamma$ case. The Lorentz invariant resulting from this operator, linear in the two polarization vectors, is $\epsilon_{\mu\nu\alpha\beta} \epsilon_1^\mu(\lambda) \epsilon_2^\nu(\lambda') Q_1^\alpha Q_2^\beta$ (times a coefficient down by α compared to the tree-level scalar case). In the pseudoscalar particle rest frame this invariant is proportional to $\epsilon_1(\lambda) \times \epsilon_2(\lambda') \cdot (Q_1 - Q_2)$, which tells us that only transverse polarizations, or equivalently, left and right helicities, are produced. Furthermore, the linear polarization vectors are perpendicular to each other. In a helicity basis, the two helicities are again identical. We expect the final decay planes to remember the vector-boson polarizations, just as in electromagnetic decay of scalar or pseudoscalar particles to two e^+e^- pairs [12]. Since a scalar parent particle gives a Lorentz-invariant combination of polarization vectors differing from that of a pseudoscalar parent, we expect the angular orientation of the final fermion decay planes to be an indicator of the parity of the parent particle.

So far, our discussion of polarization has concerned itself only with vector polarization. In fact, since the polarization of the gauge bosons cannot be directly mea-

sured, a true description of the gauge-boson polarization requires a density matrix; the vector polarization is just the diagonal part of the general density matrix. The density matrix for an off-shell vector boson is a 4×4 matrix. Since our calculation couples the gauge boson to a conserved final-state current (in the massless fermion approximation), only the “physical” 3×3 sector contributes. When either gauge boson is put on shell and treated as an observable particle, as with the OGBOS approximation, the correlations contained in the off-diagonal elements are lost. Of course, all of the correlations implied by the density matrix formalism are contained in the exact result of Eqs. (A17)–(A21), which we use.

Let us define the azimuthal asymmetry parameters α_1 and α_2 according to the formula

$$\frac{d\Gamma}{d\phi} = \frac{\Gamma}{2\pi} [1 + \alpha_1(V) \cos\phi + \alpha_2(V) \cos 2\phi]. \quad (1)$$

ϕ is the angle between the two planes, where each plane is defined by the two fermion momentum vectors resulting from the decay of a virtual or real gauge boson, as measured in the four-fermion c.m. system (c.m.s.) (i.e., the Higgs boson rest frame). ϕ is invariant under boosts in the direction of the momentum of either gauge boson. V stands for either the WW decay mode or the ZZ mode. The expressions for $\alpha_1(V)$ and $\alpha_2(V)$ for scalar Higgs decay are given in Eqs. (A17) and (A18). $\alpha_1(V)$ is a parity-violating asymmetry and $\alpha_2(V)$ is parity conserving. We show in Fig. 3 the asymmetry parameters as a function of the Higgs mass M_H for the decays $H \rightarrow ZZ \rightarrow d\bar{d}s\bar{s}$ and $H \rightarrow WW \rightarrow u\bar{d}s\bar{c} + \bar{u}d\bar{s}c$. For convenience, we have chosen final states such that identical fermions, requiring antisymmetrization, do not occur, and such that interference between the two- W graph and the two- Z graph does not occur. It is seen that the asymmetries are largest for the intermediate-mass Higgs and peak near the threshold values $M_H = 2M_W, 2M_Z$ for $\alpha_{1,2}(W), \alpha_{1,2}(Z)$, respectively.

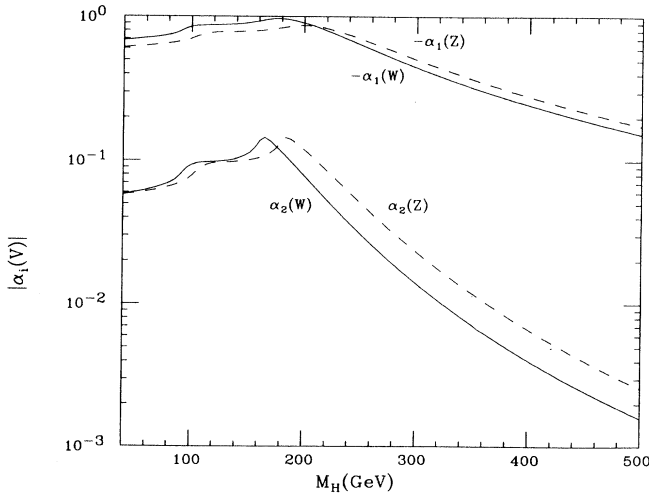


FIG. 3. Asymmetry parameters $\alpha_i(V)$, $i=1,2$, $V=Z,W$, for the decays $H \rightarrow Z^*Z^* \rightarrow d\bar{d}s\bar{s}$ and $H \rightarrow W^*W^* \rightarrow u\bar{d}s\bar{c}$ vs the Higgs mass M_H . Only $\alpha_1(Z)$ is dependent on the final state; for $u\bar{u}c\bar{c}$ ($e^+e^-\mu^+\mu^-$) it is lower than $d\bar{d}s\bar{s}$ by a factor of 0.53 (0.029).

At threshold the two V 's are nearly on shell and at rest, so the three nonzero helicity amplitudes are equal and the off-diagonal density matrix elements are maximized. In particular, the parity-violating asymmetry $\alpha_1(V)$ can be of order 1 for the intermediate-mass Higgs, and may provide a clean consistency check on the scalar nature of the decaying Higgs particle. In comparison, from Fig. 3 we see that the parity-conserving asymmetry is reduced by an order of magnitude or more.

Unfortunately, the large asymmetry α_1 is difficult to determine experimentally. The azimuthal angle may be written as $\cos\phi = \hat{n}_1 \cdot \hat{n}_2$, where $\hat{n}_{1,2}$ are the normals to the two WW or ZZ decay planes. To determine these normals, an experimenter must have charge and possibly flavor identification of the emitted leptons and/or jets. An $f \leftrightarrow \bar{f}$ ambiguity results in a $\hat{n} \leftrightarrow -\hat{n}$ or $\phi \leftrightarrow \pi - \phi$ ambiguity, and washes out the $\cos\phi$ asymmetry α_1 . On the other hand, the $\cos 2\phi$ term is even under this ambiguity, but α_2 is small except near VV threshold.

The asymmetries have been calculated before for on-shell W 's and Z 's [18], and for the QCD background process $gg, q\bar{q} \rightarrow ZZ \rightarrow 4f$ [19]. Applying the NWA to our more general results, Eqs. (A17) and (A18), or referring to the literature, one finds simple expressions:

$$\begin{aligned} \alpha_1(\text{on-shell } V\text{'s}) &= \frac{9\pi^2}{16} \left[\frac{C_R - C_L}{C_R + C_L} \right] \\ &\times \frac{M_V^2(M_H^2 - 2M_V^2)}{(M_H^2 - 2M_V^2)^2 + 8M_V^4}, \quad (2) \\ \alpha_2(\text{on-shell } V\text{'s}) &= \frac{2M_V^4}{(M_H^2 - 2M_V^2)^2 + 8M_V^4}, \quad V=W, Z. \quad (3) \end{aligned}$$

At threshold $\alpha_2(V) = \frac{1}{6}$ (evident in our figure); above threshold $\alpha_2(W)$ and $\alpha_2(Z)$ fall rapidly [asymptotically, as $(M_V/M_H)^4$] to less than 2% at $M_H \geq 300$ GeV. What is new in our calculations are the below threshold results: $\alpha_2(V)$ falls as M_H moves below the VV threshold, but slowly. When kinematics require one (two) V off shell, the asymmetry is $\approx 10\%$ (7%). For $\alpha_1(V)$, the threshold value is $(3\pi^2/32)[(C_R - C_L)/(C_R + C_L)]$. C_R and C_L are given in the Appendix. For the $V=W$ case (where parity violation is maximal, and $C_L=1, C_R=0$), $\alpha_1(W) = -3\pi^2/32 = -0.925$, nearly providing a zero in $d\Gamma/d\phi$ at $\cos\phi=1$. Extremization of $\alpha_1(V)$ with respect to M_H reveals that $|\alpha_1(V)|$ achieves its maximum value a bit above threshold, at $M_H = 2.35M_V$, i.e., at 188 (214) GeV for the W (Z) boson. This slight displacement is also evident in our figure. The above threshold falloff is not so rapid as for α_2 , going asymptotically as $(M_V/M_H)^2$. The below threshold falloff for α_1 is also weaker than for α_2 , dropping by 15% (30%) when one (two) V 's are kinematically moved off shell.

The asymmetries arise from interference among the possible $H \rightarrow V^{(*)}V^{(*)}$ helicity amplitudes. In terms of helicity amplitudes, the dependence of α_1 and α_2 on M_H is qualitatively easy to understand. Only interferences between ± 1 helicities and zero helicities contribute to α_1 ,

while only interferences between ± 1 helicities and ± 1 helicities contribute to α_2 . At threshold, all helicity states are equally populated and the relative interferences are maximized. For an off-shell V , the longitudinal mode is slightly more populated than the transverse mode, reducing the relative interference and thereby, the asymmetries. Above threshold, the transverse modes are greatly suppressed relative to the longitudinal mode, asymptotically as $(M_V/M_H)^2$, and so the asymmetries α_1 and α_2 fall as $(M_V/M_H)^2$ and $(M_V/M_H)^4$, respectively.

As may be seen from Eqs. (A17)–(A20), the asymmetry coefficients are independent of the final state *except for* $\alpha_1(Z)$. $\alpha_1(Z)$ is maximized when $Z^*Z^* \rightarrow$ two down-type quark pairs. For each up-type quark pair in the final state $\alpha_1(Z)$ is reduced by 0.73, for each charged-lepton pair by a factor of 0.17. In fact it is easy to see that $\alpha_1(V)$ is maximized when the $Vf\bar{f}$ coupling is purely chiral (either left handed or right handed) so that parity violations are maximal, and goes to zero for a coupling that is pure vector or axial vector.

The nearness of $\sin^2\theta_W$ to the “magic” value $\frac{1}{4}$ means that the vector coupling of the Z to a charged-lepton pair is nearly zero; this in turn means that the asymmetry $\alpha_1(Z)$ with a l^+l^- in the final state is nearly zero. This circumstance is most unkind, since the $Z \rightarrow l^+l^-$ mode has the best signature, both in terms of beating backgrounds, and beating the $\pm\hat{n}$ ambiguity. Prospects for reconstruction of the Higgs and its decay planes are better at e^+e^- machines than at hadron colliders.

As explained earlier, a CP -odd pseudoscalar meson does not couple to the longitudinal V s. Accordingly, it has a vanishing α_1 , but a maximal and negative α_2 value of $-\frac{1}{4}$ [18]. Such would be the asymmetries for a technipion, for example.

Incidentally, it is just this angular orientation of decay planes that was used to definitely determine the parity of the neutral pion thirty years ago [13]. Perhaps after extraordinary effort physics history will repeat itself. Or perhaps other observables, such as the fermion-antifermion laboratory energy asymmetries E_+/E_- or averaged rest-frame polar angles [20], will prove more useful.

IV. HIGGS-BOSON DECAY TO FOUR FERMIONS INCLUDING A SINGLE TOP-QUARK

The coupling of the standard model Higgs boson to a fermion scales as the fermion mass over the electroweak VEV, ~ 250 GeV. Therefore, unless a fermion is heavy on the scale of the W or Z , its coupling to the Higgs is negligible. Here we consider the modification of our decay rate to four fermions when fermion masses are included. We take one fermion to be massive, and continue to neglect the other fermion masses [21]. The relevant example we consider is the decay of a Higgs boson with mass above single top-quark threshold but below $t\bar{t}$ threshold. The decay mode is $H \rightarrow$ top (mass m_t) plus three light (on the scale of the W boson, the b quark qualifies) fermions. In models where the Higgs is generated dynamically as a scalar $t\bar{t}$ bound state [22], or where the top and Higgs masses are tuned to cancel divergences

[23], the Higgs mass is expected to lie in the range $[m_t, 2m_t]$. We also note that the branching ratio of toponium to a Higgs in this mass range is expected to be a few percent via the $H\gamma$ channel. However, toponium is not expected to exist if m_t exceeds about 140 GeV, since then the top-quark lifetime is shorter than the bound-state formation time. Thus, if the $t\bar{t}$ threshold exceeds the Higgs mass, then $H \rightarrow$ single top may offer the best hope for extracting the $Ht\bar{t}$ coupling.

In addition to the graph of Fig. 1(a) already considered, there is the additional graph of Fig. 1(b), proportional to the $Ht\bar{t}$ coupling. Since Z bosons conserve flavor and therefore cannot produce a single top, the only gauge boson contributing in Fig. 1(a) is the W . For improved accuracy, we keep the mass of the b quark in the phase space, although it is omitted in the matrix element.

The expression for the width is presented in Eqs. (A1)–(A6). The width for the process $H \rightarrow WW \rightarrow t\bar{b}s\bar{c} + \bar{t}b\bar{s}c$ for various values of m_t/M_H is displayed in Fig. 4. Single but not double production of top quarks requires $0.5 < m_t/M_H < 1.0$, and various choices are indicated in the figure. From direct CDF top mass limits [4] and from radiative correction limits [5], $89 < m_t < 182$ GeV at 95% C.L. In our analysis, we relax the C.L. and assume that $m_t < 250$ GeV absolutely. For comparison, we include the massless limit ($m_t/M_H = 0$) and the $H \rightarrow b\bar{b}$ width in Fig. 4. Were the Higgs mass above $t\bar{t}$ threshold, the $H \rightarrow t\bar{t}$ width would be the $b\bar{b}$ curve scaled up by $\beta^{3/2}(m_t/m_b)^2$, where $\beta = \sqrt{1 - 4m_t^2/M_H^2}$. The massless limit describes, for example, the process $H \rightarrow WW \rightarrow u\bar{d}s\bar{c} + \bar{u}d\bar{s}c$, and is roughly 25% of the $H \rightarrow WW$ width. One can see that for $m_t/M_H \simeq 0.5$ (precisely at $t\bar{t}$ threshold) the partial width for $H \rightarrow t\bar{b}s\bar{c} + \bar{t}b\bar{s}c$ is reduced by only a factor of 10 or less compared to the massless limit for $M_H \sim 200$ –500

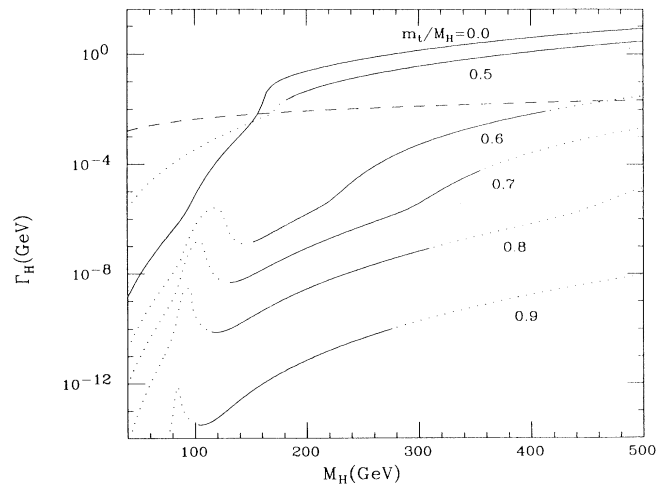


FIG. 4. $\Gamma(H \rightarrow t\bar{b}s\bar{c} + \bar{t}b\bar{s}c)$ and the massless limit $\Gamma(H \rightarrow u\bar{d}s\bar{c} + \bar{u}d\bar{s}c)$ vs M_H for constant values of M_t/M_H . The latter is roughly 25% of the $H \rightarrow WW$ width. The dotted lines correspond to regions excluded by the standard model top-quark bounds $89 < m_t < 250$ GeV. The dashed line corresponds to $\Gamma(H \rightarrow b\bar{b})$; we have not incorporated QCD corrections here, so the true $b\bar{b}$ width may be reduced as much as 50% [2].

GeV. For larger values of m_t/M_H , the partial width falls off rapidly. The ratio m_t/M_H determines how far off shell the virtual top quark is, and so determines the qualitative features of the rate. Figure 5 amply demonstrates this strong sensitivity. Starting at $m_t/M_H=0.4$ ($M_H=400$ GeV), the rate for $H \rightarrow t\bar{b}s\bar{c} + \bar{t}b\bar{s}c$ drops by $\sim 10^3$ at $m_t/M_H=0.55$. For decreasing values of M_H and fixed m_t/M_H , the drop is increasingly more severe due to diminishing phase space. If $m_t/M_H=0.6$ and $M_H > 200$ GeV, $\Gamma(H \rightarrow t\bar{b}s\bar{c} + \bar{t}b\bar{s}c)/\Gamma(H \rightarrow \tau^+\tau^-) \sim 1$, which implies a drastic reduction, since $H \rightarrow \tau^+\tau^-$ is well known to be a rare decay mode.

An important question to consider at this point is the relative magnitude of the couplings that contribute to the partial width. For large m_t , one would guess that the Yukawa contribution should be significant. This relationship is indeed demonstrated in Fig. 6; the three curves show the separate partial-width contributions arising from the Yukawa (Y), gauge (G), and Yukawa + gauge (Y+G) terms including the interference. The two graphs of Fig. 1 are individually gauge invariant so the separation into Y and G is meaningful. In Fig. 6, m_t/M_H is chosen to be 0.6, so $89 \leq m_t \leq 250$ GeV confines $150 \leq M_H \leq 420$ GeV as the physically relevant region. One can observe that Γ_Y is the dominant contribution for this range of M_H by an order of magnitude over Γ_G . At fixed M_H , Γ_Y will dominate even more for larger values of m_t/M_H .

The structure of the curves can be understood as follows: In the gauge amplitude [Fig. 1(a)] the intermediate W connecting to $t\bar{b}$ is kinematically allowed to venture on shell when $M_H > M_W > m_t + m_b$. In Fig. 6 this occurs for $M_W < M_H < 125$ GeV, and we see structure in Γ_G in this region. In the gauge and Yukawa amplitudes the intermediate W connecting the massless $q\bar{q}$ pair is kinematically allowed on shell when $M_H > M_W + m_t + m_b$. In Fig.

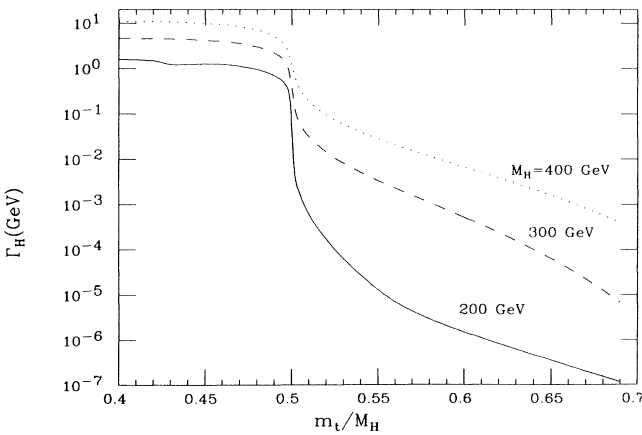


FIG. 5. $\Gamma(H \rightarrow t\bar{b}s\bar{c} + \bar{t}b\bar{s}c)$ vs m_t/M_H for fixed $M_H=200, 300, 400$ GeV. The sharp drop in Γ_H across the $H \rightarrow t\bar{t}$ threshold ($m_t/M_H=0.5$) for increasing values of m_t/M_H is due to increasing top-quark virtuality. In the range $2m_t < M_H$ the width shown is just equal to $2\Gamma(H \rightarrow t\bar{t})/B(t \rightarrow b\bar{s}c)$.

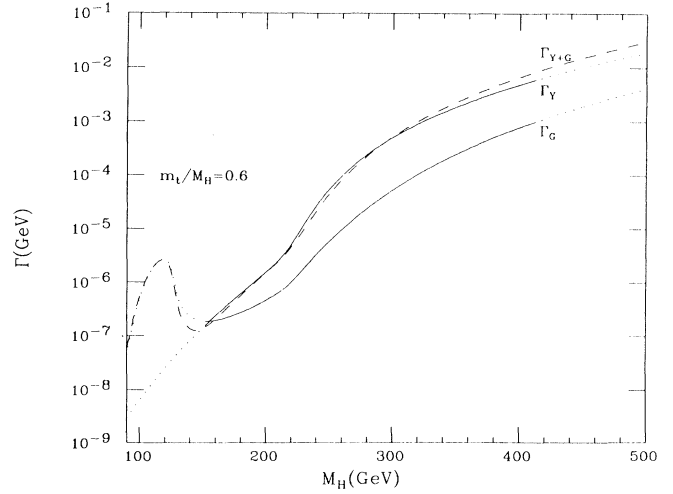


FIG. 6. $\Gamma_i(H \rightarrow t\bar{b}s\bar{c} + \bar{t}b\bar{s}c)$ vs M_H , where $i = Y, G$, and $Y+G$ refer to the Yukawa, gauge, and total (including the interference term) contributions to the partial width, respectively: Here, $m_t/M_H=0.6$.

6 this occurs for $M_H > 215$ GeV, and we see a sharp rise in both amplitudes at this value.

V. SIGNATURE AND BACKGROUND

The final states for $H \rightarrow t\bar{b}W^{(*)} \rightarrow bW^{(*)}\bar{b}W^{(*)}$ will be the same as those from the QCD process $gg \rightarrow t\bar{t} \rightarrow bW^{(*)}\bar{b}W^{(*)}$, thus making the $H \rightarrow t3f$ mode difficult to extract at a hadron collider. The signal-to-background issue here is quite similar to the well-known difficulties in extracting an above-threshold $H \rightarrow t\bar{t}$ signal from a QCD background. In fact, within the top mass resolution expected at the CERN Large Hadron Collider (LHC) and SSC detectors [24], the $\bar{b}W^{(*)}$ accompanying the single top may well mimic an associated \bar{t} . With a $bW^{(*)}$ /associated-top misidentification, the signature difficulties are identical for the $H \rightarrow$ single top and the $H \rightarrow t\bar{t}$ possibilities. However, unlike the $H \rightarrow t\bar{t}$ branching ratio, the $H \rightarrow$ single top branching ratio is small, making signal extraction much more difficult.

What may be fruitful at a hadron collider is to trigger on $t\bar{t}$ produced in association with Higgs bosons. The dominant Higgs inclusive production mechanism below $M_H = 500$ GeV is gluon-gluon fusion, which yields a cross section of ≈ 40 pb at SSC energies ($\sqrt{s} = 40$ TeV), fairly flat for $M_H \leq 500$ GeV. The $Ht\bar{t}$ cross section at SSC energies, also dominated by the gluon-gluon fusion mechanism, is ≈ 4 pb at $M_H = 150$ GeV, falling to ≈ 0.3 pb at $M_H = 500$ GeV; it is rather independent of the top mass in the range of our interests. Thus the loss in event rate is a factor of only $\approx 10-130$; on the order of 10^4 $Ht\bar{t}$ events per year may be expected assuming the standard SC integrated luminosity of 10^4 pb $^{-1}$ /SSC yr (10^7 sec). The $Ht\bar{t}$ cross section at the LHC ($\sqrt{s} = 16$ TeV) is down from that of the SSC by an order of magnitude or more (a function of masses). However, the higher design luminos-

ity at the LHC may argue for a number of $Ht\bar{t}$ events comparable to the SSC. It has been shown recently [25] that triggering on an isolated secondary lepton, e or μ , from decay of the associated t or \bar{t} renders discovery of the intermediate-mass Higgs feasible at the SSC, via the rare decay mode $H \rightarrow \gamma\gamma$ ($B \simeq 10^{-3}$). In an analogous fashion, one may hope that extraction of the rare decay mode presented here, $H \rightarrow t\bar{b}W^{(*)}$, may also be feasible in association with a $t\bar{t} \rightarrow$ isolated l^\pm trigger. A $pp \rightarrow t\bar{t}(H \rightarrow t\bar{b}W^{(*)})X$ event [or above $t\bar{t}$ threshold, the $pp \rightarrow t\bar{t}(H \rightarrow t\bar{t})X$ event] would lead to a spectacular number of high- p_T jets and leptons. If the Higgs is not reconstructible in the single top mode, then an excess of spectacular events may be the only signal from the mode. Possibly helpful for signal enhancement is the fact that W 's from the Higgs decay chain will be predominantly longitudinally polarized [26], whereas "background" W 's produced by light quarks will be transversely polarized.

The order α_s^4 $pp \rightarrow t\bar{t}t\bar{t}$ QCD background to our process has been calculated recently [27]. The result is $\sigma_{\text{QCD}}(pp \rightarrow t\bar{t}t\bar{t}X) = 1, 0.4, 0.2,$ and 0.07 pb at the SSC for $m_t = 100, 140, 170, 200$ GeV; and $0.1, 0.3, 0.008,$ and 0.003 pb for the same m_t values at the LHC. Thus, at either the SSC or the LHC, $\sigma(pp \rightarrow t\bar{t}HX) / \sigma_{\text{QCD}}(pp \rightarrow t\bar{t}t\bar{t}X) \simeq 0.3-50$, depending on the Higgs and top masses in the range of our interest ($100 \leq M_H \leq 500$ GeV, $90 \leq m_t \leq 250$ GeV). Thus a $B \geq 10^{-2}$ in the $H \rightarrow t\bar{b}W^{(*)}$ mode may in principle be observable. From Fig. 4, if $M_H > 160$ GeV, then $m_t < 0.55M_H$ appears to be needed to obtain such a branching ratio. A concern is that there is no obvious signature distinguishing the $t\bar{t}$ from $H \rightarrow t\bar{b}W^{(*)}$ from the second $t\bar{t}$ in the QCD signal; all tops will tend to be produced near threshold. The extra combinatoric possibilities available with four tops is also problematic. A Monte Carlo simulation is required to quantitatively determine detection capabilities for the $H \rightarrow t\bar{b}W^{(*)}$ mode.

At a future e^+e^- collider, it may prove possible to probe a smaller $B(H \rightarrow t\bar{b}W)$, and hence a larger m_t/M_H ratio, if the integrated luminosity is sufficiently high, and if the $t\bar{t}$ and $t\bar{t}t\bar{t}$ backgrounds are more controllable. The associated $Z+H$ and/or WW fusion cross section for production of a 100-GeV SM Higgs is 0.30, 0.14, and 0.24 pb for the values $\sqrt{s} = 200, 500,$ and 1 TeV, while for a 200-GeV Higgs it is roughly 0.1 pb over the range $\sqrt{s} = 500$ GeV to $\sqrt{s} = 1$ TeV, and for a 500-GeV Higgs it is 0.03 pb at $\sqrt{s} = 1$ TeV [2]. Thus, with $10 \text{ fb}^{-1}/\text{yr}$ of luminosity, 300–3000 Higgs events per year are anticipated. A $100 \text{ fb}^{-1}/\text{yr}$ machine has even been discussed, for which the rates are larger by a factor of 10. We conclude that branching ratios as small as 10^{-3} may be detectable.

Finally, we comment that if M_H exceeds $t\bar{t}$ threshold, as opposed to the mass range $m_t < M_H < 2m_t$ considered in this paper, then

$$\frac{\sigma(pp \rightarrow t\bar{t}(H \rightarrow t\bar{t})X)}{\sigma_{\text{QCD}}(pp \rightarrow t\bar{t}t\bar{t}X)} \sim (0.3-50) \times B(H \rightarrow t\bar{t}), \quad (4)$$

which suggests that the $Ht\bar{t}$ coupling may be experimen-

tally accessible if $B(H \rightarrow t\bar{t})$ exceeds 10^{-2} . Using SM formulas, one finds $B(H \rightarrow t\bar{t}) \simeq \Gamma(H \rightarrow t\bar{t}) / \Gamma(H \rightarrow t\bar{t}, ZZ, W^+W^-) = r(1-r)^{3/2} / [1 + r(1-r)^{3/2}]$, where $r \equiv 4m_t^2 / M_H^2$ and terms of order M_Z/M_H have been neglected. This branching ratio can be as large as 30% (at $r = 0.4$ or $m_t \sim M_H/3$), clearly warranting further study of this mode. As with the subthreshold process $H \rightarrow tX$, a Monte Carlo simulation is required to determine signal viability.

VI. FERMIOPHOBIA, GAUGEOPHOBIA, AND FERMIOPHILIA

Given the possibility that gauge-boson masses and fermion masses may arise from different mechanisms, one can imagine scalar fields (i) with couplings to fermions suppressed relative to the SM values m_f/v_{EW} , (ii) with couplings to WW and ZZ suppressed relative to the SM values $g^2 v_{\text{EW}}/2$ and $g^2 v_{\text{EW}}/(2 \cos^2 \theta_W)$, respectively, and (iii) with enhanced couplings to the fermions. We will label these scalars fermiophobic, gaugeophobic, and fermiophilic. One can easily invent models of each kind and find examples of each kind in the literature. We have already mentioned the $\phi \rightarrow -\phi$ fermiophobic scalar. Any scalar in an SU(2) representation other than doublet will also be fermiophobic since the SU(2) invariance then forbids the $\phi \bar{\Psi}_L \Psi_R$ operator.

The $\phi^2 WW, \phi^2 ZZ, (\phi^* \vec{\partial} \phi)W,$ and $(\phi^* \vec{\partial} \phi)Z$ couplings are fixed by the gauge coupling g . However, the ϕWW and ϕZZ couplings are proportional to $g^2 \langle \phi \rangle$. Accordingly, the latter are suppressed if $\sqrt{2} \langle \phi \rangle$ is less than $v_{\text{EW}} = 246$ GeV. In fact, the measured value of the ρ parameter tells us that VEV's of representations larger than doublet are much smaller than v_{EW} , so scalars from representations larger than doublet are gaugeophobic as well as fermiophobic. Higgs doublets may themselves be gaugeophobic, since in a multi doublet model, $v_{\text{EW}}^2 = \sum_{\text{doublets}} v_D^2$ sums the positive contribution from each doublet. Further models abound. As mentioned earlier, in models which conserve CP in the Higgs and gauge-boson sectors, the pseudoscalar Higgs bosons are gaugeophobic [2]. In general two-doublet models, the charged Higgs and the single CP -odd Higgs are gaugeophobic [2].

Fermiophilic scalars may result from multiscalar mixing. A well-known example is the general two-doublet model, in which some Yukawa couplings are enhanced by VEV ratios, while others are suppressed (fermiophobia again) by the inverse ratio. (Particularly well-motivated two-doublet models are the minimal supersymmetric model invented to stabilize the weak scale and the Peccei-Quinn model [28] invented to solve the strong CP problem.) There is also the possibility of scalar fields in representations which do not get a VEV. These non-Higgs scalars would have no tree-level ϕWW or ϕZZ couplings (i.e., gaugeophobic) and arbitrary Yukawa couplings (fermiophobic or fermiophilic). Such "extra" scalars have been invoked in many theoretical contexts [29].

Finally, we mention hybrid models where the VEV of a fundamental scalar field generates one mass scale, while other masses arise from a condensate or from mixing

with heavy singlet fermions [30]. Such models incorporate the best attributes of technicolor or fermion singlet masses with the simple attributes of Higgs physics, but with an increase in field content and a decrease in aesthetics. What is clear is that when a Higgs particle is finally discovered, its branching ratios will be very revealing. From the SM branching ratios of Fig. 2 in Ref. [11], one may infer the dominant decay modes of nonstandard Higgs bosons: for a neutral fermiophobic Higgs omit the two-fermion and two-gluon modes, for a neutral gaugeophobic Higgs omit the four-fermion, WW , and ZZ modes. Ignoring the loop- and mixing-induced $H \rightarrow f\bar{f}$ rate and the two-loop $H \rightarrow gg$ rate, one learns that the dominant decay mode for a fermiophobic Higgs is $\gamma\gamma$ for $M_H \leq 80$ GeV and four fermions for $M_H > 80$ GeV (via W^*W^* for $80 \leq M_H \leq 100$ GeV, via W^*W for $100 \text{ GeV} \leq M_H < 2M_W$, and via WW above the production threshold). Estimates of the rates for the induced $\bar{f}f$ and gg modes require calculations within a specific model. For a heavy gaugeophobic Higgs, the $t\bar{t}$ mode is dominant over the WW mode.

At the SSC machine with energy $\sqrt{s} \sim 40$ TeV, the $gg \rightarrow$ top-quark loop $\rightarrow H$ chain is expected to be the dominant production mechanism for a standard Higgs with $M_H \leq 5m_t$ (as here). However, a fermiophobic Higgs may in fact have as its dominant production mode WW fusion or $W^* \rightarrow WH$ with a smaller production rate. At an e^+e^- machine, the standard Higgs is expected to be produced via $Z^* \rightarrow Z + H$ for \sqrt{s} up to $400 \text{ GeV} + 0.6M_H$, and by WW fusion at higher \sqrt{s} [2]. A gaugeophobic Higgs would have a suppressed production rate, either in association with $b\bar{b}$ or $t\bar{t}$ (if kinematically allowed) or via a top-quark loop.

Let us now discuss changes in the rate for $H \rightarrow t +$ three fermions when the Higgs is nonstandard. Let $v/\sqrt{2}$ denote the VEV of the nonstandard scalar multiplet. Then the HWW coupling is $g^2v/2$ and the $H\bar{t}t$ coupling is an arbitrary constant g_Y . If we make the reasonable assumption that all Higgs fields couple to top quarks with the same sign, then $m_t = \sum_{\text{scalars}} g_Y v/\sqrt{2}$ provides the constraint $g_Y < \sqrt{2}m_t/v$; we write $g_Y = \sqrt{2}\xi m_t/v$, $0 \leq \xi \leq 1$. If $v < v_{EW}$, the Higgs is gaugeophobic; if $\xi/v < 1/v_{EW}$, the Higgs is fermiophobic; and if $\xi/v > 1/v_{EW}$, the Higgs is fermiophilic. If H is in fact a scalar without a VEV, then setting v equal to zero yields the appropriate result: decoupling from W^+W^- and an arbitrary coupling to $t\bar{t}$. The rate for nonstandard $H \rightarrow t +$ three fermions in terms of v and ξ can be obtained from Fig. 6: Γ_Y scales as $(\xi v_{EW}/v)^2$, Γ_G scales as $(v/v_{EW})^2$, and the interference term scales simply as ξ . For a truly gaugeophobic Higgs, Γ_Y is the total width, while for a truly fermiophobic Higgs, Γ_G is the total width.

VII. SUMMARY

We have presented the tree decay of the SM Higgs boson to four fermions, including the possibility of a single massive fermion in the final state in order to explore the potentially large Yukawa contribution to the decay rate. In the massless limit, we have demonstrated that if both

gauge bosons are off shell, the rate is considerably reduced. If one gauge boson can go on shell, it will, and therefore the OGBOS approximation is valid for an intermediate-mass Higgs. We have also explored how a measurement of the angular correlation of the decay planes of the final-state fermions may lead to a determination of the intrinsic parity of the Higgs, even if $M_H < 2M_W$.

Next, we have shown that for a Higgs mass below $t\bar{t}$ threshold, the decay rate to a single top quark is generally dominated by the Yukawa coupling, and thus tests the SM mechanism for fermion mass generation. For a Higgs just below the $t\bar{t}$ threshold, the single top rate is only $\sim 10^{-1}$ down from the massless mode where the gauge coupling is the only contribution. As m_t/M_H grows, the overall rate is dramatically reduced. It is evident (see, e.g., Fig. 4) that the $H \rightarrow t\bar{t}W^{(*)}$ process remains competitive in rate with other potentially detectable rare decay modes such as $H \rightarrow \gamma\gamma, Z\gamma, b\bar{b}, \tau^+\tau^-$ over much of the allowed range of $M_H, m_t/M_H$. At a hadron collider, the signal to background is enhanced by triggering on $pp \rightarrow t\bar{t}HX$ signatures, making $H \rightarrow$ single top possibly observable if $2m_t \lesssim 1.1M_H$; a Monte Carlo simulation is needed to quantitatively compare the signal to the $O(\alpha_s^4) t\bar{t}t\bar{t}$ QCD background. [Prospects appear brighter for measuring $\Gamma(H \rightarrow t\bar{t})$ via $pp \rightarrow t\bar{t}HX$, should M_H exceed $2m_t$.] It appears that $H \rightarrow$ single top may have a better chance for detection at a future high-energy, high-luminosity e^+e^- collider, where branching ratios as small as 10^{-3} , i.e., $2m_t \lesssim 1.2M_H$, may be measurable.

Finally, we have shown that the rate for Higgs \rightarrow single top is a sensitive measure of any ‘‘nonstandardness’’ in either the Higgs-gauge boson and/or the Higgs-fermion sectors of the true theory. We have discussed the implications of ‘‘nonstandardness’’ in these sectors for the general issue of fermion and gauge-boson mass generation.

ACKNOWLEDGMENTS

We have benefited from discussions with Bill Marciano, Jack Gunion, Howie Haber, and Wendell Holladay. This work was supported in part by U.S. Department of Energy Grants Nos. DE-FG05-85ER40226, DE-AC02-76-ER022789, and DE-FG03-84ER40168. Part of this work was carried out at the Aspen Center for Physics.

APPENDIX

The Lorentz-invariant matrix element for particle decay to a four-body final state depends on five independent variables. We find it convenient to use as variables the invariant mass of each fermion pair connected by a common fermion line (there are two of these), the polar angle of the particle momentum with respect to the pair momentum direction evaluated in the pair center-of-mass frame (there are two of these), and the azimuthal angle describing the orientation of one plane defined by paired fermion momenta relative to the plane defined by the oth-

er paired momenta (there is one of these). For the case with all massless final-state particles, where only graph 1(a) contributes, the first four of these variables are just the virtual W or Z boson invariant masses and the fer-

mion momentum direction relative to its parent W or Z momentum direction evaluated in the W or Z boson rest frame. The Lorentz-invariant phase space in terms of these variables is

$$\int dX_{\text{LIPS}} = \int_{(m_t+m_b)^2}^{M_H^2} dQ_1^2 \int_0^{(M_H - \sqrt{Q_1^2})^2} dQ_2^2 \int_0^{2\pi} d\phi \int_{-1}^1 d \cos\theta_1 \int_{-1}^1 d \cos\theta_2 \frac{\lambda^{1/2}(M_H^2, Q_1^2, Q_2^2) \lambda^{1/2}(Q_1^2, m_t^2, m_b^2)}{2^8 M_H^2 Q_1^2 (2\pi)^6}, \quad (\text{A1})$$

where $\lambda(a, b, c) = a^2 + b^2 + c^2 - 2(ab + bc + ca)$ is the usual triangle function. (An alternate choice of the five independent phase-space variables is discussed in [31]). The width is

$$\Gamma(H \rightarrow (t\bar{b} + \bar{t}b) + f\bar{f}) = \frac{1}{M_H} \int d^4 X_{\text{LIPS}} \sum_{\text{spin}} |\mathcal{M}|^2, \quad (\text{A2})$$

where

$$\sum_{\text{spin}} |\mathcal{M}|^2 = \sum_{\text{spin}} (\mathcal{M}_a \mathcal{M}_a^* + \mathcal{M}_b \mathcal{M}_b^* + 2 \text{Re} \mathcal{M}_a \mathcal{M}_b^*) \quad (\text{A3})$$

expresses the summation over the squares of the amplitudes from Figs. 1(a) and 1(b) and the interference of the two amplitudes. The expressions for these squared matrix elements are

$$\sum_{\text{spin}} \mathcal{M}_a \mathcal{M}_a^* = 3^n g^6 M_W^2 B_W(Q_1^2) B_W(Q_2^2) \left[4f \cdot t \bar{f} \cdot \bar{b} - 2 \left[\frac{m_t}{M_W} \right]^2 [\bar{f} \cdot \bar{b} f \cdot Q_1 + f \cdot \bar{b} \bar{f} \cdot Q_1 - \frac{1}{4} Q_2^2 (Q_1^2 - m_t^2)] + \frac{m_t^2 (Q_1^2 - m_t^2)}{M_W^4} (f \cdot Q_1 \bar{f} \cdot Q_1 - \frac{1}{4} Q_1^2 Q_2^2) \right], \quad (\text{A4})$$

$$\sum_{\text{spin}} \mathcal{M}_b \mathcal{M}_b^* = \frac{3^n g^6 m_t^2}{M_W^2} B_W(Q_2^2) [(M_H^2 - 2P \cdot t)^2 + (m_t \Gamma_t)^2]^{-1} [\bar{f} \cdot \bar{b} (2f \cdot Pt \cdot P - M_H^2 f \cdot t)], \quad (\text{A5})$$

$$\begin{aligned} 2 \text{Re} \sum_{\text{spin}} \mathcal{M}_a \mathcal{M}_b^* = & -2 \frac{3^n g^6 m_t^2}{M_W^2} [(M_H^2 - 2P \cdot t)^2 + (m_t \Gamma_t)^2]^{-1} B_W(Q_1^2) B_W(Q_2^2) \\ & \times \{ [(M_W^2 - Q_1^2)(M_H^2 - 2P \cdot t) + M_W \Gamma_W m_t \Gamma_t] \\ & \times [2M_W^2 f \cdot P \bar{f} \cdot \bar{b} - Q_1 \cdot \bar{f} (P \cdot Q_1 f \cdot \bar{b} - P \cdot \bar{b} Q_1 \cdot f) \\ & - Q_1 \cdot \bar{b} (P \cdot \bar{f} Q_1 \cdot f - P \cdot Q_1 f \cdot \bar{f}) - \frac{1}{2} Q_1^2 (P \cdot f \bar{b} \cdot \bar{f} + P \cdot \bar{b} f \cdot \bar{f} - P \cdot \bar{f} \bar{b} \cdot f)] \\ & + \frac{1}{2} [M_W \Gamma_W (M_H^2 - 2P \cdot t) + m_t \Gamma_t (Q_1^2 - M_W^2)] (2Q_1 \cdot \bar{f} + Q_1^2) \epsilon^{\alpha\beta\mu\nu} P_\alpha \bar{f}_\beta Q_{1\mu} \bar{b}_\nu \}, \quad (\text{A6}) \end{aligned}$$

where $g = |e|/\sin\theta_W$ and $B_V(Q^2) = [(Q^2 - M_V^2)^2 + M_V^2 \Gamma_V^2]^{-1}$ is the vector-boson Breit-Wigner factor ($V = W$ or Z). For convenience, we take M_Z and Γ_Z to be 91 and 2.5 GeV, respectively, and M_W and Γ_W to be 80 and 2.1 GeV, respectively. The weak mixing angle is taken to be $\sin^2\theta_W = 0.23$. In all of our rate equations, 3^n is a color factor, with n being the number of quark-antiquark pairs in the final state.

Note that we have retained the b -quark mass in the phase space. However, we have omitted it in the above matrix elements since to the same order in m_b/M_W there is a further graph given by exchanging the b and t quarks in Fig. 1(b), which we have not included. We take $m_b = 4.7$ GeV. For the top width Γ_t , we have summed the following expression over $(f, \bar{f}') = (u, \bar{d}), (c, \bar{s}), (e, e^+), (\nu_\mu, \mu^+), (\nu_\tau, \tau^+)$:

$$\Gamma(t \rightarrow b W^{(*)} \rightarrow b f \bar{f}') = \frac{3^n m_t g^4}{3\pi^3 \times 2^{10}} \int_{2\sqrt{r}}^{1+r} dx_b \frac{\sqrt{x_b^2 - 4r} [3(1+r)x_b - 2x_b^2 - 4r]}{[(1-x_b+r) - \hat{M}_W^2]^2 + \hat{\Gamma}_W^2 \hat{M}_W^2}, \quad (\text{A7})$$

where $x_b = 2E_b/m_t$, $r = m_b^2/m_t^2$, and $\hat{M}_W, \hat{\Gamma}_W = M_W/m_t, \Gamma_W/m_t$, respectively.

It is not difficult to analytically integrate out the light fermion pair. The resulting expression depends on three variables, which we choose to be the paired fermion invariant masses (two of these) and twice the dot product of the Higgs four-momentum (P) with the heavy fermion four-momentum (t); we call this invariant variable $\xi = 2P \cdot t$. The Lorentz-invariant phase space is

$$\int dX_{\text{LIPS}} = \frac{1}{2^6 (2\pi)^5 M_H^2} \int_{(m_t+m_b)^2}^{M_H^2} dQ_1^2 \int_0^{(M_H - \sqrt{Q_1^2})^2} dQ_2^2 \int_{\xi_-}^{\xi_+} d\xi, \quad (\text{A8})$$

with

$$\xi_{\pm} \equiv \frac{1}{2Q_1^2} [(M_H^2 + Q_1^2 - Q_2^2)(Q_1^2 + m_t^2 - m_b^2) \pm \lambda^{1/2}(Q_1^2, m_t^2, m_b^2) \lambda^{1/2}(M_H^2, Q_1^2, Q_2^2)] . \quad (\text{A9})$$

A technical difficulty arises at this point. As m_b is turned on from zero, ξ_- decreases, therein going out of the physical region for the $m_b^2=0$ matrix element. We have cured this disease by setting $\xi_- \equiv \xi_-(m_b=0)$, $\xi_+ \equiv \xi_-(m_b=0) + [\xi_+(m_b \neq 0) - \xi_-(m_b \neq 0)]$.

We find, for the squared matrix element, in the $m_b=0$ limit,

$$\begin{aligned} \sum_{\text{spin}} \mathcal{M}_a \mathcal{M}_a^* &= \frac{3^n \pi g^6 M_W^2}{24} B_W(Q_1^2) B_W(Q_2^2) \\ &\times \left[2Q_2^2(2Q_1^2 - \xi) - 2(\xi - Q_1^2 - m_t^2)(\xi - M_H^2 - m_t^2) \right. \\ &\quad \left. + \frac{2m_t^2}{M_W^2} [(M_H^2 + m_t^2 - Q_2^2 - \xi)(Q_1^2 + Q_2^2 - M_H^2) + 2Q_2^2(Q_1^2 - m_t^2)] + \frac{m_t^2}{2M_W^4} (Q_1^2 - m_t^2) \lambda(M_H^2, Q_1^2, Q_2^2) \right] , \end{aligned} \quad (\text{A10})$$

$$\begin{aligned} \sum_{\text{spin}} \mathcal{M}_b \mathcal{M}_b^* &= \frac{3^n \pi g^6 m_t^2}{48 M_W^2} B_W(Q_2^2) [(M_H^2 - \xi)^2 + (m_t \Gamma_t)^2]^{-1} \\ &\times \{ \xi [(Q_2^2 - Q_1^2)(2M_H^2 + m_t^2 - 2Q_2^2) - M_H^2 m_t^2] + M_H^2 [(M_H^2 + m_t^2)(Q_1^2 + m_t^2) - 2Q_2^2 Q_1^2] + \xi^2 (Q_1^2 - 2Q_2^2) \} , \end{aligned} \quad (\text{A11})$$

$$\begin{aligned} 2 \operatorname{Re} \sum_{\text{spin}} \mathcal{M}_a \mathcal{M}_b^* &= -\frac{\pi}{12} 3^n g^6 m_t^2 [(M_H^2 - \xi)^2 + (m_t \Gamma_t)^2]^{-1} [(M_W^2 - Q_1^2)(M_H^2 - \xi) + M_W \Gamma_W m_t \Gamma_t] B_W(Q_1^2) B_W(Q_2^2) \\ &\times \left[\xi \left[Q_1^2 - 2Q_2^2 - M_H^2 + \frac{Q_1^2}{2M_W^2} (M_H^2 + Q_2^2 - Q_1^2) \right] \right. \\ &\quad \left. + \frac{1}{2M_W^2} \{ -M_H^2 Q_1^2 (M_H^2 - Q_1^2 - Q_2^2) + m_t^2 [(Q_1^2 - Q_2^2)^2 - M_H^2 (Q_1^2 + Q_2^2)] \} \right. \\ &\quad \left. + M_H^2 (M_H^2 + m_t^2) + (Q_1^2 - Q_2^2)(2Q_2^2 - M_H^2 - m_t^2) \right] . \end{aligned} \quad (\text{A12})$$

The limit of all massless final-state particles is easily obtained from the above equations. For the V^*V^* intermediate state ($V=W$ or Z), the result is

$$\begin{aligned} \Gamma(H \rightarrow V^*V^* \rightarrow f_1 \bar{f}'_1 f_2 \bar{f}'_2) &= \frac{4 \times 3^n g^6 M_V^2}{2M_H} \int d^4 X_{\text{LIPS}} [C_L(f_1 \cdot f_2)(\bar{f}'_1 \cdot \bar{f}'_2) + C_R(f_1 \cdot \bar{f}'_2)(f_2 \cdot \bar{f}'_1)] B_V(2f_1 \cdot \bar{f}'_1) B_V(2f_2 \cdot \bar{f}'_2) . \end{aligned} \quad (\text{A13})$$

For the $V=W$ mode, the chiral couplings are just

$$C_L = 1 , \quad C_R = 0 . \quad (\text{A14})$$

For the $V=Z$ mode, they are

$$\cos^6 \theta_W C_L = \frac{1}{2} (v_1^2 + a_1^2)(v_2^2 + a_2^2) + 2v_1 v_2 a_1 a_2 \quad (\text{A15})$$

and

$$\cos^6 \theta_W C_R = \frac{1}{2} (v_1^2 + a_1^2)(v_2^2 + a_2^2) - 2v_1 v_2 a_1 a_2 , \quad (\text{A16})$$

with $v_i = (T_{3R} + T_{3L} - 2Q \sin^2 \theta_W)_i$ and $a_i = (T_{3R} - T_{3L})_i$, where T_{3L} and T_{3R} are the weak isospin eigenvalues of the left- and right-helicity fermions and Q is the fermion electric charge in units of $|e|$. Integrating these expressions over the two polar angles leads to the following expressions for the asymmetry parameters [defined in Eq. (1) in the main text]:

$$\alpha_1(V) = \left[\frac{C_R - C_L}{C_R + C_L} \right] \frac{9\pi^2}{32D} \int_0^{M_H^2} dQ_1^2 \int_0^{(M_H - \sqrt{Q_1^2})^2} dQ_2^2 \lambda^{1/2}(M_H^2, Q_1^2, Q_2^2) B_V(Q_1^2) B_V(Q_2^2) (M_H^2 - Q_1^2 - Q_2^2) \sqrt{Q_1^2 Q_2^2} , \quad (\text{A17})$$

$$\alpha_2(V) = \frac{1}{D} \int_0^{M_H^2} dQ_1^2 \int_0^{(M_H - \sqrt{Q_1^2})^2} dQ_2^2 \lambda^{1/2}(M_H^2, Q_1^2, Q_2^2) B_V(Q_1^2) B_V(Q_2^2) Q_1^2 Q_2^2, \quad (\text{A18})$$

with

$$D = \frac{1}{2} \int_0^{M_H^2} dQ_1^2 \int_0^{(M_H - \sqrt{Q_1^2})^2} dQ_2^2 \lambda^{1/2}(M_H^2, Q_1^2, Q_2^2) B_V(Q_1^2) B_V(Q_2^2) [8Q_1^2 Q_2^2 + (M_H^2 - Q_1^2 - Q_2^2)^2]. \quad (\text{A19})$$

The final-state dependence of the asymmetry $\alpha_1(Z)$ is given by

$$\left[\frac{C_R - C_L}{C_R + C_L} \right] = - \frac{4v_1 v_2 a_1 a_2}{(v_1^2 + a_1^2)(v_2^2 + a_2^2)}. \quad (\text{A20})$$

In the massless fermion limit, further integration of the general expression (A13) may be done analytically, leading to

$$\begin{aligned} \Gamma(H \rightarrow V^* V^* \rightarrow f_1 \bar{f}'_1 f_2 \bar{f}'_2) \\ = \frac{g^6 m_V^2 3^n}{2^9 \times 9 \times M_H^3 (2\pi)^5} (C_L + C_R) \int_0^{M_H^2} dQ_1^2 \int_0^{(M_H - \sqrt{Q_1^2})^2} dQ_2^2 \lambda^{1/2}(M_H^2, Q_1^2, Q_2^2) \\ \times [8Q_1^2 Q_2^2 + (M_H^2 - Q_1^2 - Q_2^2)^2] B_V(Q_1^2) B_V(Q_2^2). \quad (\text{A21}) \end{aligned}$$

When kinematics allow one or both vector boson(s) to go on shell, it will. Then the appropriate limits of our general expressions are found by applying the NWA, $B_V(Q^2) \rightarrow \pi \delta(Q^2 - M_V^2) / M_V \Gamma_V$ (times a possible symmetry factor of 2, as explained in the text). As a check on formulas (A17)–(A21), we apply the NWA to each vector boson and obtain known on-shell results. The on-shell values of the asymmetries of $\alpha_1(V)$ and $\alpha_2(V)$ are given in the text; the on-shell values of Eq. (A21) are just

$$\Gamma(H \rightarrow W^+ W^- \rightarrow f_1 \bar{f}'_1 f_2 \bar{f}'_2) = \Gamma(H \rightarrow W^+ W^-) B(W^+ \rightarrow f_1 \bar{f}'_1) B(W^- \rightarrow f_2 \bar{f}'_2) \quad (\text{A22})$$

and

$$\Gamma(H \rightarrow ZZ \rightarrow f_1 \bar{f}'_1 f_2 \bar{f}'_2) = 2\Gamma(H \rightarrow ZZ) B(Z \rightarrow f_1 \bar{f}'_1) B(Z \rightarrow f_2 \bar{f}'_2). \quad (\text{A23})$$

Similarly, the NWA replacement $B_V(Q^2) \rightarrow \pi \delta(Q^2 - M_V^2) / M_V \Gamma_V$ in Eqs. (A1)–(A6) and (A8)–(A12) yields the rate for $\Gamma(H \rightarrow i\bar{b}W) B(W \rightarrow f\bar{f}')$.

-
- [1] M. Chanowitz and M. Gaillard, Nucl. Phys. **B261**, 379 (1985).
- [2] See, for example, J. F. Gunion, H. E. Haber, G. L. Kane, and S. Dawson, *The Higgs Hunters' Guide* (Addison-Wesley, Redwood City, CA, 1990), and references therein.
- [3] M. Davier, in *Proceedings of the Joint International Lepton-Photon Symposium and Europhysics Conference on High Energy Physics*, Geneva, Switzerland, 1991, edited by S. Hegarty, K. Potter, and E. Quercigh (World Scientific, Singapore, 1992). The new ALEPH bound is $M_{H_{SM}} > 54$ GeV. ALEPH Collaboration, D. Decamp *et al.*, Phys. Lett. B **246**, 306 (1990); DELPHI Collaboration, P. Abreu *et al.*, Nucl. Phys. **B342**, 1 (1990); L3 Collaboration, B. Adeva *et al.*, Phys. Lett. B **257**, 452 (1991); OPAL Collaboration M. Z. Akrawy *et al.*, *ibid.* **253**, 511 (1991).
- [4] CDF Collaboration, F. Abe *et al.*, Phys. Rev. Lett. **64**, 147 (1990).
- [5] For recent analysis see P. Langacker and M. Luo, Phys. Rev. D **44**, 817 (1991), and references therein.
- [6] M. Veltman, Acta Phys. Pol. B **8**, 475 (1977).
- [7] J. Ellis, in *Proceedings of the Joint International Lepton-Photon Symposium and Europhysics Conference on High Energy Physics* [3]; T. G. Rizzo, Mod. Phys. Lett. A **6**, 2947 (1991). See also W. Hollik, lectures delivered at the 21st G.I.F.T., Santander, Spain, 1990 (unpublished), and in Proceedings of the 13th Warsaw Symposium on Elementary Particles, Kazimierz, Poland, 1990 (unpublished).
- [8] H. E. Haber and R. Hempfling, Phys. Rev. Lett. **66**, 1815 (1991); J. Ellis, G. Ridolfi, and F. Zwirner, Phys. Lett. B **257**, 83 (1991); **262**, 477 (1991); R. Barbieri, M. Frigeni, and F. Caravaglios, *ibid.* **258**, 167 (1991); J. L. Lopez and D. V. Nanopoulos, *ibid.* **266**, 397 (1991); Y. Okada, M. Yamaguchi, and T. Yanagida, Prog. Theor. Phys. **85**, 1 (1991). See also P. H. Chankowski, S. Pokorski, and J. Rosiek, Phys. Lett. B **274**, 191 (1992).
- [9] J. F. Gunion, G. L. Kane, and J. Wudka, Nucl. Phys. **B299**, 231 (1988).
- [10] W.-Y. Keung and W. J. Marciano, Phys. Rev. D **30**, 248 (1984).
- [11] V. Barger, G. Bhattacharya, T. Han, and B. A. Kniehl, Phys. Rev. D **43**, 779 (1991).
- [12] C. N. Yang, Phys. Rev. **77**, 722 (1950); N. M. Kroll and W. Wada, *ibid.* **98**, 1355 (1955).
- [13] N. P. Samios, R. Plano, A. Prodel, M. Schwartz, and J. Steinberger, Phys. Rev. Lett. **3**, 524 (1959); Phys. Rev. **126**, 1844 (1961). The nonobservation of the process $\pi^- + d \rightarrow 2n + \pi^0$, expected to be highly suppressed if the π^0 has odd parity, provided earlier circumstantial evidence for the π^0 's parity: See W. Chinowsky and J. Steinberger, Phys. Rev. **100**, 1476 (1955).
- [14] For example, in technicolor models, the technifermions condense to generate a Higgs mechanism, while the fermions acquire their masses from a separate "extended" technicolor sector. See E. Farhi and L. Susskind, Phys.

- Rep. **74**, 2777 (1981).
- [15] A two-doublet model with one of the doublets yielding "fermiophobic" Higgs particles was discussed some time ago by H. E. Haber, G. L. Kane, and T. Sterling, Nucl. Phys. **B161**, 553 (1979), Appendix B.
- [16] T. J. Weiler, in *Collider Physics: Current Status and Future Prospects*, Proceedings of the Eighth Vanderbilt International Conference on High Energy Physics, Nashville, Tennessee, 1987, edited by J. Brau and R. S. Panvini (World Scientific, Singapore, 1988).
- [17] C. N. Yang, Phys. Rev. **77**, 242 (1950).
- [18] M. J. Duncan, G. L. Kane, and W. W. Repko, Nucl. Phys. **B272**, 517 (1986); J. R. Del'Aquila and C. A. Nelson, Phys. Rev. D **33**, 80 (1986); **93**, 93 (1986); C. A. Nelson, *ibid.* **37**, 1220 (1988); T. Matsuura and J. J. van der Bij, Z. Phys. C **51**, 259 (1991).
- [19] Matsuura and van der Bij [18].
- [20] M. J. Duncan, Phys. Lett. B **179**, 393 (1986); Duncan, Kane, and Repko [18].
- [21] The inverse process, t quark \rightarrow Higgs + light fermion + (W or W^*), has been considered by T. G. Rizzo, Phys. Rev. D **35**, 1067 (1987); V. Barger and W.-Y. Keung, Phys. Lett. B **202**, 393 (1988).
- [22] W. A. Bardeen, C. T. Hill, and M. Lindner, Phys. Rev. D **41**, 1647 (1990), and references therein. Bubble sums yield a weakly bound top-quark condensate with $M_H \sim 2m_t$; renormalization-group improved sums yield a more strongly bound result of $M_H \sim 1.1m_t$.
- [23] P. Osland and T. T. Wu, Phys. Lett. B **391**, 315 (1992), use cancellation of certain divergences to fix $M_H \sim 190$ GeV and $m_t \sim 120$ GeV.
- [24] F. E. Paige, Brookhaven National Laboratory Report No. 45828, 1991 (unpublished).
- [25] W. J. Marciano and F. E. Paige, Phys. Rev. Lett. **66**, 2433 (1991); J. F. Gunion, Phys. Lett. B **261**, 51 (1991).
- [26] In the Higgs-boson decay chain, both the Higgs boson and top quark decay to W 's. For $M_H^2 \gg M_W^2$, the ratio of Higgs-produced longitudinal W 's to transverse W 's is $M_H^4/8M_W^4$, while for top-produced W 's, the same ratio is $m_t^2/2M_W^2 + O(m_b^2/M_W^2)$. These ratios are easy to understand when the equivalence theorem is invoked.
- [27] V. Barger, A. L. Stange, and R. J. N. Phillips, Phys. Rev. D **44**, 1987 (1991); **45**, 1484 (1992).
- [28] R. Peccei and H. Quinn, Phys. Rev. D **16**, 1791 (1977).
- [29] Most recently, charged singlet scalars have been invented to generate a large transition magnetic moment for the light neutrinos. See S. M. Barr and E. M. Friere, Phys. Rev. D **43**, 2989 (1991), and references therein.
- [30] E. H. Simmons, Nucl. Phys. **B312**, 253 (1989); **B324**, 315 (1989); A. Kagan and S. Samuel, Phys. Lett. B **252**, 605 (1990); Int. J. Mod. Phys. A **7**, 1123 (1992).
- [31] Kroll and Wada [12]; T. Miyazaki and E. Takasugi, Phys. Rev. D **8**, 2051 (1973).